Multi-Ring Circular Transmission Line Model for Ultralow Contact Resistivity Extraction

Hao Yu, Marc Schaekers, Tom Schram, Erik Rosseel, Koen Martens, Steven Demuynck, Naoto Horiguchi, Kathy Barla, Nadine Collaert, Kristin De Meyer, *Fellow*, *IEEE*, and Aaron Thean

***Abstract*—Accurate determination of contact resistivities (ρ_c) below 1×10^{-8} Ω·cm² is challenging. Among the frequently applied Transmission Line Models (TLM), Circular TLM (CTLM) has a simple process flow, while refined TLM (RTLM) has a high ρ_c accuracy at the expense of a more complex fabrication. In this letter, we will present a novel model—multi-ring CTLM (MR-CTLM), which combines the advantages of a simple process and a high ρ_c extraction resolution. We fabricated ultralow-ρ_c Ti/n-Si contacts and demonstrated the capability of MR-CTLM to extract the ρ_c as low as 6.2×10^{-9} Ω·cm² with high precision.**

***Index Terms*—Contact resistance, transmission line model, circular transmission line model, simulation**

I. Introduction

For the 10 nm technology node and beyond, ultralow contact resistivities (ρ_c), far below 1×10^{-8} Ω·cm², are required for high-performance devices [1]. Therefore, efforts have focused on accurate ρ_c extraction models [2-5].

A ρ_c test structure with simple process and high accuracy has long been pursued [6-10]. The circular transmission line model (CTLM) is known for its simple processing [8-10]. But the metal resistance of the large electrodes of CTLM compromises its ρ_c resolution [2]. The refined transmission line model (RTLM) is a novel model that shows a high ρ_c accuracy due to its effective preclusion of the metal impact [5,12,13]. However, RTLM requires a more complex processing than CTLM.

In this work, we will first briefly review the CTLM and the RTLM and highlight their features. Next, we will present the Multi-Ring CTLM (MR-CTLM), which not only inherits the simple fabrication scheme from CTLM but also has a ρ_c accuracy comparable to RTLM. We will experimentally demonstrate the high ρ_c resolution and sensitivity of the MR-CTLM for ρ_c values below 1×10^{-8} Ω·cm².

II. Experiments

Both CTLM and MR-CTLM samples were fabricated on 300 mm lightly doped p-type Si wafers. A 50 nm Si with in-situ P doping was epitaxially grown on top of the Si wafer. An ultrahigh P concentration of 1.9×10^{21} cm^{-3} was achieved in the epitaxial Si layer [11]. After the epitaxy, some of the samples received a 2-pulse 1200 °C 0.25 ms laser dynamic surface anneal (DSA) to increase the dopant activation. Next, a ~180 nm SiO_2/SiN/SiO_2 dielectric stack was deposited across the wafer. CTLM and MR-CTLM patterns were defined by lithography. The opening of the dielectric stack—the exposure of the Si substrate—was performed by two selective dry etches and one dip in diluted HF. Then a 5 nm Ti layer was sputter deposited, followed by a liner (TiN/TaN/Ta) deposition. 800 nm Cu was deposited on the liner by plating. Chemical-mechanical planarization (CMP) was performed until ~160 nm Cu remained. After the CMP, top surface of the dielectric stack in CTLM and MR-CTLM was also exposed. An 8nm SiC layer was deposited across the wafer to prevent the Cu oxidation. Samples were measured with an HP4156c parameter analyzer.

III. CTLM and RTLM

We first compare CTLM and RTLM in terms of the process difficulty and ρ_c accuracy. CTLM and RTLM structures are shown in Fig. 1: equipotential distributions are simulated by Lump Model [2]. The dimensions of CTLM and RTLM in Fig. 1 are identical to those in [2] and [5]. The parameters used in Fig.1 are listed in the caption, where R_s and R_m are the sheet resistances of the highly doped semiconductor surface and the metal, respectively. The ρ_c and R_s settings in Fig. 1 imply a highly doped layer of 50-200 nm—a typical condition for a low ρ_c study. The small R_m corresponds to a 100-200 nm lowly resistive metal layer.

Process difficulty: Except for CTLM [9,10], most of TLMs, including RTLM, require a lateral electrical isolation—such as a mesa etch—to prevent the lateral spreading of the current in the substrate. For this reason, CTLM normally requires one less step of lithography than RTLM. Compared with RTLM, CTLM has thus a shorter and simpler fabrication.

ρ_c accuracy: Both CTLM and RTLM are micrometer-scale structures. With the modern process, these 10^2-10^4 μm² structures can be fabricated with high reproducibility. Between

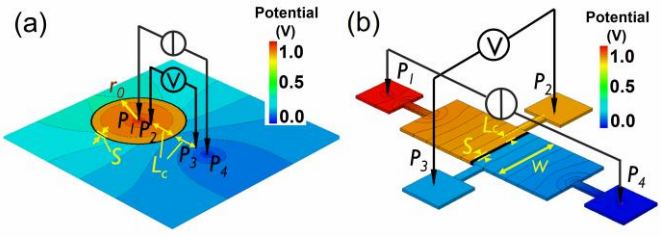

Fig. 1 Equipotential distributions of (a) CTLM and (b) RTLM based on Lump Model simulation. P_1-P_4 illustrate the placement positions of the current source and voltage detector probes. S is the spacing of the metal electrodes. L_c is the effective metal electrode length. In CTLM, inner radius r_0 = 100 μm and L_c = 60 μm; In RTLM, width W = 25 μm and L_c = 3 μm. For both CTLM and RTLM, ρ_c = 1×10^{-8} Ω·cm², R_s = 100 Ω/sq, R_m = 0.2 Ω/sq and S = 1 μm.

Manuscript submitted April 20, 2015. This work was supported by imec's Core program on LOGIC DEVICES.

H. Yu, K. Martens, and K. De Meyer are with the Department of Electrical Engineering, Katholieke Universiteit (K.U.), 3001 Leuven, Belgium, and also with imec, 3001 Leuven, Belgium, (e-mail: hao.yu@imec.be).

M. Schaekers, T. Schram, S. Demuynck, E. Rosseel, N. Collaert, N. Horiguchi, A. Thean and K. Barla are with imec, 3001 Leuven, Belgium.

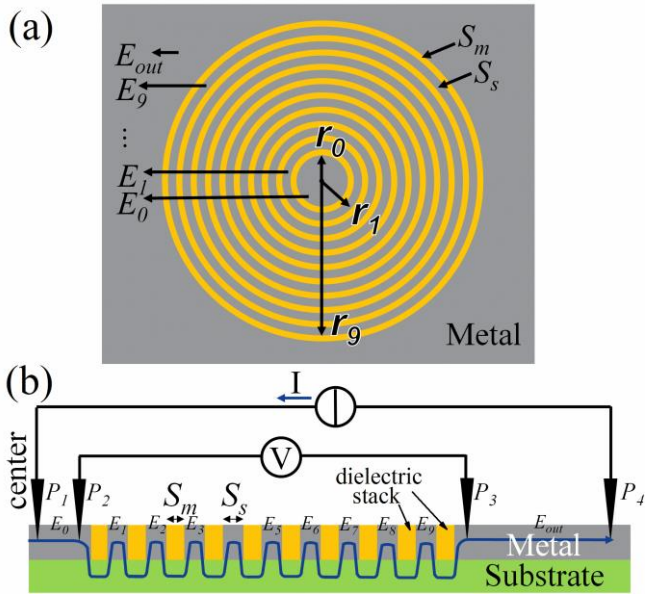

Fig. 2 Schematic a) top view and b) section view of MR-CTLM. 10 CTLMs are connected in series. r_0-r_9 are the inner radii of the serial CTLMs. E_0, E_1-E_9, and E_{out} are labels of the inner electrode, the ring electrodes, and the outer electrode, respectively. S_m is the spacing of electrodes. S_s is the width of each metal ring. In this work, S_m ranges from 0.35 μm to 10 μm, S_s =10 μm, r_0 = 30 μm and r_i (i = 1, 2, ... 9) can be calculated by $r_i = r_0 + i * (S_s + S_m)$. In a realistic measurement, P_1 is put at the cener of E_0 of the MR-CTLM; the distance between P_1 and P_4 is 300 μm; P_2 and P_3 are put close to the ring edges.

CTLM and RTLM, the most significant difference that impacts the ρ_c extraction accuracy is the metal resistance. In this aspect, RTLM is superior to CTLM because of its small electrode length (see Fig.1). This metal impact can be illustrated by a calculation as follows. In both CTLM and RTLM (the circular correction of CTLM [6] is neglected for simplicity), the contact resistance R_c is approximated by [2]

$$R_c = R_s L_t \coth(L_c/L_t) + R_m(L_c - L_t) \quad (1)$$

$$L_t = \sqrt{\rho_c/R_s} \quad (2)$$

where L_t is the transfer length and L_c is the electrode length. For large-scale TLMs, L_c>>L_t, and (1) can be simplified to

$$R_c = R_s L_t + R_m L_c \quad (3)$$

where R_mL_c stands for the parasitic metal electrode resistance, while R_sL_t is the effective contact resistance from which ρ_c is extracted. The R_mL_c/R_sL_t ratio is thus an indication of how much the ρ_c extraction is impacted by the metal electrode resistance: for a sensitive measurement, this ratio should be far below 1. Taking the parameters in Fig.1 for instance, R_mL_c/R_sL_t equals 1.2 for the CTLM but equals 0.06 for the RTLM. The R_mL_c/R_sL_t ratio difference between CTLM and RTLM simply results from different L_c. For CTLM, it is feasible to put the voltage detector probes closer to the ring to reduce L_c and use the method described in [2] to include the metal resistance in ρ_c extraction. But this requires a high precision of probe placement. For the aforementioned reasons, low ρ_c around 1×10^{-8} Ω·cm^2 with low data variance have been reported with RTLM by several groups [5,12,13], but has been only scarcely reported with CTLM [2].

In summary, CTLM and RTLM show a tradeoff between the fabrication complexity and the ρ_c accuracy. This is the reason why some groups use CTLM for the first round of ρ_c screening, but apply RTLM for ultralow ρ_c extraction [12, 13].

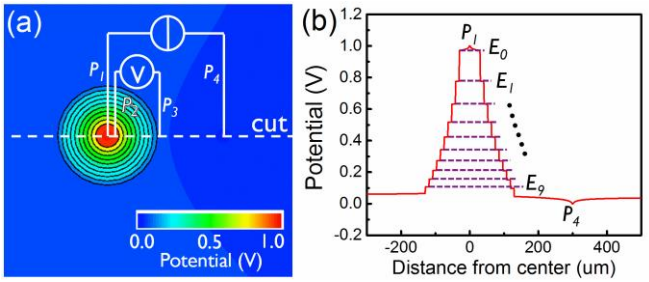

Fig. 3 (a) Equipotential distributions in MR-CTLM based on Lump Model simulation. The potential profile along "cut" is shown in (b). P_1-P_4 indicate probe positions. Dimension of MR-CTLM is identical to those in Fig. 2. ρ_c = 1×10^{-8} Ω·cm^2, R_s = 100 Ω/sq, R_m = 0.2 Ω/sq and S_m = 1 μm. In (b), E_0 is the inner electrode of MR-CTLM; E_1-E_9 are the 9 annular electrodes; horizontal dashed lines are guides to the eye to compare the potential across each metal electrode.

IV. MULTI-RING CTLM

Both the simple processing of CTLM and the high ρ_c accuracy of RTLM are attractive for low ρ_c studies. Interestingly, we can combine both advantages in MR-CTLM. As shown in Fig. 2, MR-CTLM is actually several CTLMs in series, which hence has an identical processflow to CTLM: only one step of lithography is needed, without the requirement of a lateral electrical isolation. Comparable to RTLM, the L_c of MR-CTLM is small—L_c = S_s/2 = 5μm in this work. MR-CTLM is thus also immune to the metal resistance impact.

A Lump Model simulation of the MR-CTLM was performed in Fig. 3 with the same parameters used in Fig. 1. Clearly, MR-CTLM has several advantages over the CTLM: (1) multiple serial rings in MR-CTLM compose a large effective resistance—the contact resistances plus the channel resistances (resistances beneath dielectric stack in Fig. 2b). Therefore, a much smaller portion of voltage drops over the metal in MR-CTLM (Fig. 3a) than that in CTLM (Fig. 1a); (2) the large effective resistance in MR-CTLM reduces the variance of ρ_c extraction and improves measurement efficiency; (3) large ratio of effective resistance to metal resistance renders MR-CTLM insensitive to small probe placement deviations; (4) for the small-spacing CTLM, the metal resistance induces an invalid equipotential assumption along the ring in the case of low ρ_c studies [2] (see Fig. 1a), while for MR-CTLM, the equipotential assumption along the rings is valid (see Fig. 3). This is because the metal resistance is negligible compared with the effective resistance in the MR-CTLM. This equipotential is a prerequisite to build a valid numerical equation for MR-CTLM with annular resistors.

In the calculation, we break the total resistance of the MR-CTLM, R_t, into R_e and R_p—the effective resistances and the parasitic metal resistances. For a 10-ring MR-CTLM (Fig. 2), since R_s>>R_m and r_i>>L_t, R_t can be calculated by [9]

$$R_t = R_e + R_p \quad (4)$$

$$R_e = \frac{R_s}{2\pi}\sum_{i=0}^{9}\left[\ln\left(\frac{r_i + S_m}{r_i}\right) + L_t\left(\frac{1}{r_i} + \frac{1}{r_i + S_m}\right)\right] \quad (5)$$

$$R_p = \frac{R_m}{2\pi}\left[\sum_{i=1}^{9}\ln\left(\frac{r_i - L_t}{r_i - S_s + L_t}\right)\right] \quad (6)$$

Normally, R_t of MR-CTLM with different S_m is measured following the probe positions illustrated in Fig.2b; R_m is derived by four-point probe measurement. Next to that, the parameters

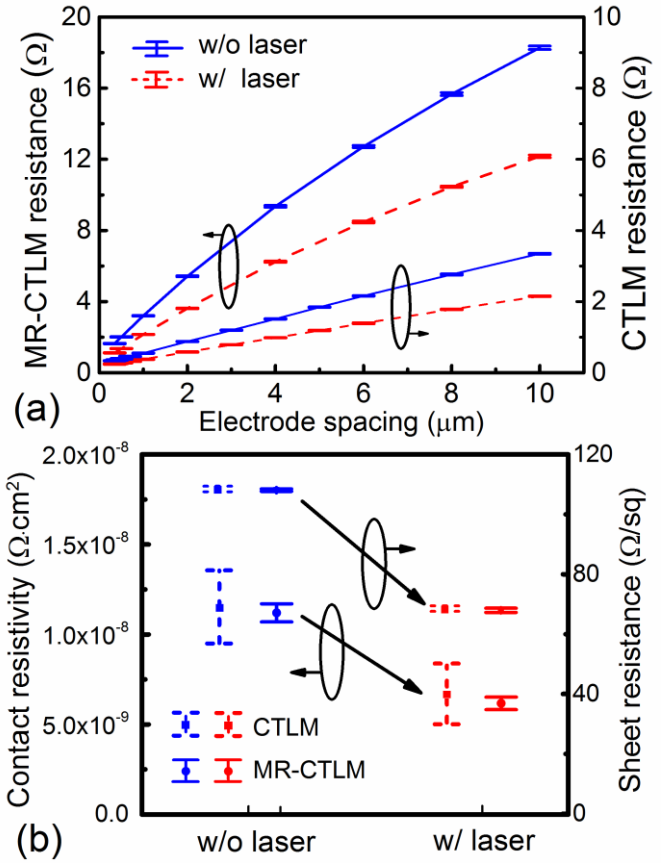

Fig. 4 (a) Measurement and fitting of Ti/n-Si R_t-S_m data of MR-CTLM and R_t-S data of CTLM. The MR-CTLM dimension is described in Fig. 2. The CTLM applied has an inner radius r_0 of 50 μm, an effective electrode length L_c of ~30 μm and a set of electrode spacing ranging from 0.35 μm to 10 μm. (b) ρ_c and R_s extracted from MR-CTLM and CTLM. MR-CTLM and CTLM fitting are both based on measurements of six chips. On each chip, MR-CTLM and CTLM were fabricated at close positions. R_m and R_T were measured chip by chip, while ρ_c and R_s were extracted by curve fitting. The solid dots and the error bars in (a) and (b) are averages and standard deviations of data, respectively.

R_s and L_t are extracted by fitting a set of R_t-S_m data using (4)-(6). Then ρ_c is derived by (2). The curve fitting with (4)-(6) can be easily handled by software, such as Matlab or Solver of Excel.

Fig. 4a illustrates the curve fitting and the parameter extraction with R_t-S_m data of the MR-CTLM. Six sets of data were measured for each condition. The small error bars in Fig. 4a show the high precision of the measurement. Ultralow ρ_c of $(6.17 \pm 0.35) \times 10^{-9}\ \Omega\cdot\text{cm}^2$ and $(1.12 \pm 0.05) \times 10^{-8}\ \Omega\cdot\text{cm}^2$ were extracted for Ti/n-Si with and without laser activation. With laser enhancement, $5\text{-}6\times10^{20}\ \text{cm}^{-3}$ out of the total $1.9\times10^{21}\ \text{cm}^{-3}$ was activated (as determined by SIMS, XRD, Hall and R_s) [11].

To verify the ρ_c and R_s extracted by MR-CTLM, we also fabricated CTLM and extracted the parameters in Fig. 4a using the method in [2]. As shown in Fig. 4b, the CTLM and the MR-CTLM gave similar ρ_c averages, but the MR-CTLM exhibited a smaller standard deviation—a better ρ_c resolution. The ρ_c resolution difference between the MR-CTLM and CTLM can be explained as follows: Firstly, measurement and fitting of each MR-CTLM are virtually performed on multiple CTLMs in series. Therefore, with MR-CTLM, ρ_c is extracted from an averaged performance of multiple CTLMs and hence has less variance than ρ_c extracted from single CTLM. Secondly, MR-CTLM has a large ratio of effective resistance to metal resistance and is much less impacted by the R_m variance than CTLM. Thirdly, for the ultralow ρ_c measurement in this work, R_T of the small-spacing CTLM is so low (< 0.5 Ω, see Fig. 4a) that the system error from the measurement tool also adds to the data variation. In contrast, R_T of MR-CTLM is augmented by the ring numbers and is thus less vulnerable to the small system errors. For these reasons, MR-CTLM shows a more promising resolution for ultralow ρ_c studies than CTLM.

In summary, we demonstrate that MR-CTLM has a high sensitivity and resolution for ultralow ρ_c below $1\times10^{-8}\ \Omega\cdot\text{cm}^2$. This high ρ_c accuracy is comparable to those reported with RTLM [5,12,13]. Moreover, same with CTLM, MR-CTLM has a simple process scheme which requires only one step of lithography and no lateral electrical isolation. Therefore, MR-CTLM is proved to be highly appealing for advanced ultralow ρ_c studies.

V. Conclusions

We propose a novel multi-ring CTLM (MR-CTLM) structure for the low ρ_c studies. MR-CTLM combines the advantages of an easy fabrication process with a high ρ_c accuracy. It is thus an ideal test vehicle for future contact studies. We built a numerical model for MR-CTLM and demonstrated its capability to extract ρ_c values as low as $6.2\times10^{-9}\ \Omega\cdot\text{cm}^2$ with high precision.

[1] *The International Technology Roadmap for Semiconductors (ITRS)*, 2013
[2] H. Yu, M. Schaekers, T. Schram, *et al.*, "A simplified method for (circular) transmission line model simulation and ultralow contact resistivity extraction", *IEEE Electron Device Lett.*, vol. 35, no. 9, pp. 957-959, Sept. 2014
[3] W. Lu, A. Guo, A. Vardi, and J. A. del Alamo, "A test structure to characterize nano-scale ohmic contacts in III-V MOSFETs", *IEEE Electron Device Lett.*, vol. 35, no. 2, pp. 178-180, Feb. 2014
[4] K. Majumdar, S. Vivekanand, C. Huffman, *et al.*, "STLM: a sidewall TLM structure for accurate extraction of ultralow specific contact resistivity", *IEEE Electron Device Lett.*, vol. 34, no. 9, pp. 1082-1084, Sept. 2013
[5] R. Dormaier and S. E. Mohney, "Factors controlling the resistance of ohmic contacts to n-InGaAs", *J. Vac. Sci. Technol. B*, vol. 30, no. 3, pp. 031209-1-031209-10, May/Jun 2012
[6] D. K. Schroder, *Semiconductor material and device characterization*, 3rd chapter, pp. 127, John Wiley & Sons, 2006
[7] H. H. Berger. "Contact resistance on diffused resistors." *Solid-State Circuits Conference. Digest of Technical Papers.1969 IEEE Internationa*. No. 117.
[8] H. Murrmann and D. Widmann, "Messung des übergangswiderstandes zwischen metall und diffusionsschicht in Si-planarelementen", *Solid-state Electronics*, 12, pp. 879-886, 1969.
[9] G. S. Marlow and M. B. Das, "The effects of contact size and non-zero metal resistance on the determination of specific contact resistance", *Solid-State Electron.*, vol. 25, no. 2, pp. 91-94, 1982
[10] G. K. Reeves, "Specific contact resistance using a circular transmission line model", *Solid-State Electron.*, vol. 23, pp. 487-490, 1980
[11] E. Rosseel, H. B. Profijt, A. Y. Hikavyy, *et al.* "Characterization of Epitaxial Si: C: P and Si: P Layers for Source/Drain Formation in Advanced Bulk FinFETs.", *ECS Trans.*, Vol. 64, No. 6, pp. 977, 2014
[12] J. D. Yearsley, J. C. Lin, E. Hwang, *et al.*, "Ultra low-resistance palladium silicide ohmic contacts to lightly doped n-InGaAs", *J. Appl. Phys*, vol. 112, pp. 054510-1-054510-8, Sept. 2012
[13] H. Miyoshi, T. Ueno, K. Akiyama, et al. "In-situ contact formation for ultra-low contact resistance NiGe using carrier activation enhancement (CAE) techniques for Ge CMOS." *VLSI Technology (VLSI-Technology): Digest of Technical Papers, 2014 Symposium on*. IEEE, 2014